A simplified GW/BSE approach for charged and

neutral excitation energies of large molecules and

nanomaterials

Yeongsu Cho,† Sylvia J. Bintrim,† and Timothy C. Berkelbach*,†,‡

†Department of Chemistry, Columbia University, New York, New York 10027, USA

‡Center for Computational Quantum Physics, Flatiron Institute, New York, New York 10010, USA

E-mail: tim.berkelbach@gmail.com

Abstract

Inspired by Grimme's simplified Tamm-Dancoff density functional theory approach [S.

Grimme, J. Chem. Phys. 138, 244104 (2013)], we describe a simplified approach to excited

state calculations within the GW approximation to the self-energy and the Bethe-Salpeter equa-

tion (BSE), which we call sGW/sBSE. The primary simplification to the electron repulsion

integrals yields the same structure as with tensor hypercontraction, such that our method has a

storage requirement that grows quadratically with system size and computational timing that

grows cubically with system size. The performance of sGW is tested on the ionization poten-

tial of the molecules in the GW100 test set, for which it differs from ab initio GW calculations

by only 0.2 eV. The performance of sBSE (based on sGW input) is tested on the excitation en-

ergies of molecules in the Thiel's set, for which it differs from ab initio GW/BSE calculations

by about 0.5 eV. As examples of the systems that can be routinely studied with sGW/sBSE, we

calculate the band gap and excitation energy of hydrogen-passivated silicon nanocrystals with

up to 2650 electrons in 4678 spatial orbitals and the absorption spectra of two large organic

dye molecules with hundreds of atoms.

1

1 Introduction

The GW approximation to the self-energy and the Bethe-Salpeter equation (BSE) are known to provide accurate charged and neutral excitation energies, respectively. $^{1-9}$ Physically, the accuracy of these methods is attributable to the use of the *screened* Coulomb interaction in many-body perturbation theory. Given their successful application to solid-state materials, they have been increasingly applied to problems in molecular chemistry, for which they have been found to be affordable approaches with reasonable accuracy. $^{10-18}$ The computational cost of *ab initio* GW/BSE calculations depends on implementation details, which yield computational timings that scale as N^3 to N^6 with system size N^{19-30} (throughout this work we exclusively consider the non-self-consistent G_0W_0 approximation but will typically refer to it as the GW approximation, for brevity). Although promising, the storage requirements and computational timing for *ab initio* GW/BSE calculations are still prohibitive for applications to very large systems or to problems requiring many calculations, such as averaging over the course of a molecular dynamics trajectory or in workflows for materials screening. The present work is concerned with reducing this cost and we will largely ignore the qualitative features or applicability of GW/BSE methods, which are well documented; we refer to the reviews presented in Refs. 31-33 for further information.

The same observations about computational costs of *ab initio* density functional theory (DFT) and time-dependent DFT (TDDFT) have led to a number of more affordable semiempirical approximations, including density functional tight-binding (DFTB), ^{34,35} extended tight-binding (xTB), ^{36–38} the simplified Tamm-Dancoff approximation/TDDFT (sTDA/sTDDFT), ^{39,40} and combinations thereof, such as TD-DFTB, ^{41,42} sTDA-xTB, ⁴³ and TDDFT+TB. ⁴⁴ These affordable, semiempirical methods have had significant impact in the field of chemical simulations, enabling ground-state and excited-state calculations of large molecules with more than one thousand atoms; for more details and specific examples, we refer the reader to a recent Perspective article. ⁴⁵ Inspired in particular by Grimme's sTDA, here we present a simplified GW/BSE approach that we call sGW/sBSE. At the heart of both approaches is an approximation to the electron repulsion integrals, which we show leads to a sGW/sBSE implementation with storage requirements that are quadratic in sys-

tem size and execution times that are cubic in system size. Because we only introduce numerical approximations, we expect sGW/sBSE to be physically appropriate for the same types of systems as *ab initio* GW/BSE, i.e., weakly to moderately correlated molecules and materials. Although sGW/sBSE results differ from *ab initio* ones by 0.1-1 eV, they can be applied to very large systems using only commodity computing resources (in fact, the results presented here are limited in size by the cost of the initial DFT calculation). In this regard, the sGW/sBSE methods are not meant to be replacements for advanced *ab initio* GW/BSE implementations that can be deployed on high-performance computing architectures. Instead, they facilitate simple, rapid, and semiquantitative calculations that are intermediate between effective-mass or related model-based approaches and fully *ab initio* approaches.

2 Theory

2.1 Integral approximations

A standard DFT calculation is first performed to yield the Kohn-Sham eigenvalues ε_p and molecular orbitals (MOs) $\psi_p(r)$. For the remainder of the manuscript, we will use i, j, k, l to index occupied MOs in the Kohn-Sham reference, a, b, c, d to index unoccupied MOs, and p, q, r, s for general MOs. In contrast to many GW/BSE implementations that utilize plane-wave basis sets, in our work the MOs are expanded in a basis of atomic orbitals (AOs) $\phi_{\mu}(r)$ or symmetrically orthogonalized AOs $\phi'_{\mu}(r)$,

$$\psi_p(r) = \sum_{\mu} \phi_{\mu}(r) C_{\mu p} = \sum_{\mu} \phi'_{\mu}(r) C'_{\mu p},$$
 (1)

where $\mathbf{C}' = \mathbf{S}^{1/2}\mathbf{C}$ and \mathbf{S} is the AO overlap matrix. The primary simplification we make is to the four-center two-electron repulsion integrals (ERIs), whose storage and manipulation is responsible for much of the cost in correlated calculations with atom-centered basis functions. Specifically, the

MO ERIs are approximated as (in 1122 notation),

$$(pq|rs) = \sum_{\mu\nu\kappa\lambda} C'_{\mu p} C'_{\kappa q} C'_{\nu r} C'_{\lambda s} (\mu\kappa|\nu\lambda)'$$

$$\approx \sum_{\mu\nu} C'_{\mu p} C'_{\mu q} C'_{\nu r} C'_{\nu s} (\mu\mu|\nu\nu)' \equiv \sum_{\mu\nu} L^{\mu}_{pq} L^{\nu}_{rs} J_{\mu\nu}$$
(2)

where $L^{\mu}_{pq} = C'_{\mu p} C'_{\mu q}$ is the orthogonalized AO component of the orbital pair density, $J_{\mu \nu} = (\mu \mu | \nu \nu)'$ is a one- or two-center Coulomb type integral in the orthogonalized AO basis, and the primed notation indicates ERIs calculated over orthogonalized AO basis functions. The above approximation recognizes that Coulomb-type ERIs $(\mu \mu | \nu \nu)'$ are typically the largest, which is also known as the zero differential overlap approximation. The O(N) one-center Coulomb integrals are evaluated exactly, $J^{(1c)}_{\mu \nu} = (\mu \mu | \nu \nu)'$, and the $O(N^2)$ two-center Coulomb integrals are approximated by the Mataga-Nishimoto-Ohno-Klopman formula, $^{46-48}$

$$J_{\mu\nu}^{(2c)} \approx \left(\frac{1}{|r_{\mu} - r_{\nu}|^2 + \eta_{\mu\nu}^{-2}}\right)^{1/2},$$
 (3)

where $\eta_{\mu\nu} = \left[J_{\mu\mu}^{(1c)} + J_{\nu\nu}^{(1c)}\right]/2$. This approximation to the two-center Coulomb integrals has the correct asymptotic behavior when $|r_{\mu} - r_{\nu}| \gg 0$ and reproduces one-center Coulomb integrals $(r_{\mu} = r_{\nu})$ when $\mu = \nu$.

Although the final algebraic structure of our ERI approximation is similar to that of the sTDA method, our specific choices are quite different. The sTDA approximation to MO ERIs follows from our Eq. (2) by first neglecting the orbital dependence of $J_{\mu\nu}$ and retaining only its atomic dependence $J_{\mu\nu} \approx J_{AB}$, which yields $(pq|rs) \approx \sum_{AB} J_{AB} q_{pq}^A q_{rs}^B$ where $q_{pq}^A = \sum_{\mu \in A} L_{pq}^{\mu}$ are pair density charges according Löwdin population analysis. In early stages of our work, we found this approximation too crude for an accurate representation of the dielectric matrix, which is why we keep the explicit AO dependence of the ERI parameterization. Next, we recall that in TDA calculations, the only MO ERIs that appear are of the Coulomb type (ij|ab) and exchange type (ia|jb) for occupied-unoccupied pairs. Within sTDA, this motivates a separate parameterization

of J_{AB} depending on whether it appears in a Coulomb or exchange-type integral (Ref. 39 further adopted a more general parameterization than our Eq. (3) and introduced four global empirical parameters). In contrast, GW/BSE calculations require many more MO ERI types, necessitating the general approximation scheme (2).

The ERI approximation (2) has the same structure as the density fitting approximation (also known as the resolution of the identity approximation), $^{49-52}$ which has been regularly used in ab initio GW/BSE implementations with atom-centered basis sets. ^{24,26–29,53,54} However, we emphasize that here the three-index tensors L_{pq}^{μ} are expressible as a product of two-index objects, the MO coefficients. Therefore, the standard density fitting procedure, requiring the calculation of two-center and three-center integrals and the solution of a system of linear equations, is completely bypassed (although we note that it may be used in the initial DFT calculation) and three-index objects need not be stored. More importantly, the second equality of Eq. (2) has the same structure as the compressed ERIs in tensor hypercontraction methods, ⁵⁵ leading to an sGW/sBSE implementation that only requires the storage of two-index objects and opportunities for reductions in the scaling of the computational time. Matrices expressed in the basis of single particle orbitals require only trivial amount of memory; for example, with 10,000 basis functions, such a matrix requires less than 1 GB of memory. The use of this approximate but efficient MO ERI compression in GW/BSE calculations is the primary novelty of this work. In contrast to other advanced implementations, the speedups enabled in the sGW/sBSE methods described in the next sections do not rely on sparsity that is only realized in asymptotic limits with localized orbitals.

2.2 Simplified GW

The GW approximation and the resulting approximate solution to the Bethe-Salpeter equation are Green's function techniques. The GW approximation is similar to the Hartree-Fock approximation, except that it uses a dynamically screened exchange interaction that accounts for the response of the other electrons upon electron addition or removal. In practice, the self-energy is commonly evaluated in a "one-shot" manner, as a correction to DFT MO energies. Within the diagonal G_0W_0

approximation, matrix elements of the self-energy operator are given by

$$\Sigma_p(\omega) = \Sigma_p^{(c)}(\omega) + \Sigma_p^{(x)} \tag{4}$$

where $\Sigma_p^{(x)}$ is the static exchange part of the self-energy (i.e., matrix elements of the nonlocal exchange potential) and $\Sigma_p^{(c)}(\omega)$ is the dynamical correlation part of the self-energy. We first consider the static exchange part and recall that hybrid functionals often provide a better starting point for G_0W_0/BSE calculations, 16,33,56 in which case matrix elements of the exchange potential are already available and can be reused for free in the evaluation of the GW self-energy (4). When the initial DFT calculation is done with a semilocal functional, then several options exist. The exchange potential matrix elements can be calculated exactly with a one-time $O(N^3)$ cost per eigenvalue or $O(n_{\rm GW}N^3)$ overall to calculate $n_{\rm GW}$ eigenvalues. Alternatively, the exchange matrix elements can be calculated according to their definition $\Sigma_p^{(x)} = -\sum_i (pi|ip)$, using the MO ERI approximation (2). In numerical tests (not shown), this was found to be a poor approximation to exchange potential matrix elements, which could not be cured by minor empirical modifications; we believe this to be a worthy topic of future study. Instead, we tested a modification to include one-center AO exchange integrals (only to be used for calculating matrix elements of the exchange potential),

$$(pi|ip) \approx \sum_{\mu\nu} L^{\mu}_{pi} L^{\nu}_{ip} J_{\mu\nu} + \sum_{\mu\neq\nu}^{(1c)} \left(L^{\mu}_{pi} L^{\nu}_{ip} + L^{\mu}_{pp} L^{\nu}_{ii} \right) K^{(1c)}_{\mu\nu}. \tag{5}$$

This improvement adds negligible computational cost with only $O(N^2)$ scaling but improves the accuracy of the exchange matrix elements. To increase the flexibility, the one-center AO exchange integrals $K_{\mu\nu}^{(1c)}$ were empirically scaled by a single parameter β_K , i.e., $K_{\mu\nu}^{(1c)} = \beta_K(\mu\nu|\mu\nu)'$, where the O(N) AO exchange-type ERIs $(\mu\nu|\mu\nu)'$ are calculated exactly. In Sec. 3.1, we will compare results obtained using this latter approximation and using exact exchange matrix elements.

The correlation part of the GW self-energy is the most time-consuming part to evaluate and is

given by

$$\Sigma_p^{(c)}(\omega) = \frac{i}{2\pi} \sum_q \int d\omega' \frac{W_{pqqp}(\omega) - (pq|qp)}{\omega - \omega' - \varepsilon_q + i\eta \operatorname{sgn}(\varepsilon_q - \mu)},\tag{6}$$

where η is a positive infinitesimal and μ is the chemical potential. The screened Coulomb interaction is

$$W(\mathbf{r}_1, \mathbf{r}_2; \omega) = \int d\mathbf{r} \varepsilon^{-1}(\mathbf{r}_1, \mathbf{r}; \omega) |\mathbf{r} - \mathbf{r}_2|^{-1}$$
(7)

where the dielectric function is

$$\varepsilon(\boldsymbol{r}_1, \boldsymbol{r}_2; \omega) = \delta(\boldsymbol{r}_1 - \boldsymbol{r}_2) - \int d\boldsymbol{r} |\boldsymbol{r}_1 - \boldsymbol{r}|^{-1} P(\boldsymbol{r}, \boldsymbol{r}_2; \omega)$$
(8)

and the independent-particle polarizability is

$$P(\mathbf{r}_{1}, \mathbf{r}_{2}; \omega) = \sum_{ia} \psi_{a}(\mathbf{r}_{1})\psi_{i}(\mathbf{r}_{1})\psi_{i}(\mathbf{r}_{2})\psi_{a}(\mathbf{r}_{2})$$

$$\times \left[\frac{1}{\omega - (\varepsilon_{a} - \varepsilon_{i}) + i\eta} - \frac{1}{\omega + (\varepsilon_{a} - \varepsilon_{i}) + i\eta}\right].$$
(9)

As mentioned above, Eq. (2) has the same structure as the density fitting approximation with $|\phi'_{\mu}(r)|^2$ playing the role of the auxiliary basis,

$$\psi_p(\mathbf{r})\psi_q(\mathbf{r}) \approx \sum_{\mu} C'_{\mu p} C'_{\mu q} |\phi'_{\mu}(\mathbf{r})|^2 = \sum_{\mu} L^{\mu}_{pq} |\phi'_{\mu}(\mathbf{r})|^2.$$
 (10)

In this nonorthogonal auxiliary basis, the dielectric function has a matrix representation $\varepsilon_{\mu\nu}(\omega) \equiv [\varepsilon(\omega)]_{\mu\nu}$ with

$$\varepsilon(\omega) = \mathbf{S}' - \mathbf{J}\mathbf{S}'^{-1}\mathbf{P}(\omega),\tag{11}$$

$$S'_{\mu\nu} = \int d\mathbf{r} |\phi'_{\mu}(\mathbf{r})|^2 |\phi'_{\nu}(\mathbf{r})|^2, \tag{12}$$

$$P_{\mu\nu}(\omega) = \int d\mathbf{r}_1 d\mathbf{r}_2 |\phi'_{\mu}(\mathbf{r}_1)|^2 P(\mathbf{r}_1, \mathbf{r}_2; \omega) |\phi'_{\nu}(\mathbf{r}_2)|^2.$$
 (13)

Rather than inverting the dielectric matrix at every frequency and numerically integrating, we use the plasmon-pole approximation. ^{7,57,58} Considering the generalized eigenvalue problem

$$\varepsilon(\omega)\mathbf{U}(\omega) = \mathbf{S}'\mathbf{U}(\omega)\lambda(\omega),\tag{14}$$

we assume $U(\omega) = U(\omega = 0)$ and that the eigenvalues can be parameterized by the form

$$\lambda_l^{-1}(\omega) = 1 + z_l \left(\frac{1}{\omega - (\omega_l - i\eta)} - \frac{1}{\omega + (\omega_l - i\eta)} \right). \tag{15}$$

The parameters z_l and ω_l are chosen to match the numerical eigenvalues $\lambda_l(\omega)$ obtained at the two frequencies $\omega = 0$ and $\omega = \varepsilon_{\rm gap}$ (i.e., the Kohn-Sham band gap). With this form, the frequency integration can be performed analytically to give

$$\Sigma_{p}^{(c)}(\omega) = \sum_{q\mu\nu} L_{pq}^{\mu} [\mathbf{S}' \mathbf{U} \boldsymbol{\Lambda}^{(q)}(\omega) \mathbf{U}^{-1} \mathbf{S}'^{-1} \mathbf{J}]_{\mu\nu} L_{qp}^{\nu}$$

$$= \sum_{ql} \left[\sum_{\mu} C'_{\mu p} C'_{\mu q} [\mathbf{S}' \mathbf{U}]_{\mu l} \right] \Lambda_{ll}^{(q)}(\omega)$$

$$\times \left[\sum_{\mu} [\mathbf{U}^{-1} \mathbf{S}'^{-1} \mathbf{J}]_{l\nu} C'_{\nu p} C'_{\nu q} \right]$$
(16)

where $\Lambda^{(q)}(\omega)$ is a diagonal matrix with elements

$$\Lambda_{ll}^{(q)}(\omega) = \frac{z_l}{\omega - \varepsilon_q - \omega_l \operatorname{sgn}(\varepsilon_q - \mu)}.$$
(17)

We calculate the GW quasiparticle energies E_p using the linearized form

$$E_p = \varepsilon_p + Z_p \left[\Sigma_p(\varepsilon_p) - \nu_{pp}^{(\text{xc})} \right]$$
 (18)

where $v_{pp}^{(xc)}$ is a diagonal matrix element of the DFT exchange-correlation potential and the renor-

malization factor is

$$Z_p = \left[1 - \left(\frac{\partial \Sigma(\omega)}{\partial \omega}\right)_{\omega = \varepsilon_p}\right]^{-1}.$$
 (19)

Using only $O(N^2)$ storage, the intermediates indicated in square brackets in Eq. (16) can be formed for each orbital p of interest in $O(N^3)$ time; the time needed to calculate $n_{\rm GW}$ eigenvalues is then $O(n_{\rm GW}N^3)$. If $O(N^3)$ storage is available, then the intermediates indicated can be calculated once and stored as a three-index object; the time needed to calculate *all* eigenvalues is then only $O(N^3)$. We emphasize that these computational savings are solely enabled by the compressed form of the ERIs (2).

2.3 Simplified BSE

Within the Tamm-Dancoff and static screening approximations, the BSE is an eigenvalue problem for the matrix

$$A_{ia,jb} = (E_a - E_i)\delta_{ij}\delta_{ab} + \alpha(ia|jb) - (ij|W|ab), \tag{20}$$

where $\alpha=2$ for singlets and 0 for triplets. Just like in simplified TDDFT,⁴⁰ the Tamm-Dancoff approximation could be removed within sBSE by including the associated space of deexcitations. Note that GW quasiparticle energies E_p are required as input to a BSE calculation; sGW energies will be used in sBSE calculations. With the integral simplification (2) and the static screening approximation to the screened Coulomb interaction (7), in sBSE we have

$$(ij|W|ab) = \sum_{\mu\nu} L^{\mu}_{ij} L^{\nu}_{ab} W_{\mu\nu} = \sum_{\mu\nu} C'_{\mu i} C'_{\nu j} C'_{\nu a} C'_{\nu b} W_{\mu\nu}$$
(21a)

$$\mathbf{W} = \mathbf{S}' \varepsilon^{-1} (\omega = 0) \mathbf{J}$$
 (21b)

Note that (ij|W|ab) has the same structure as the bare (ij|ab), with $W_{\mu\nu}$ replacing $J_{\mu\nu}$, and that $W_{\mu\nu}$ can be built simply by matrix multiplication, requiring only quadratic storage and cubic CPU time. We discuss further computational costs of sBSE below.

For comparison, we also provide results obtained by the simplified TDA approach, ³⁹ which is

a structurally identical eigenvalue problem for the matrix

$$A_{ia,ib} = (\varepsilon_a - \varepsilon_i)\delta_{ii}\delta_{ab} + \alpha(ia|jb) - a_x(ij|ab), \tag{22}$$

where a_x is the fraction of exact exchange included in the DFT functional. We will present results obtained with the original ERI approximations of Ref. 39 (which we will call sTDA) as well as with our ERI approximation (2) (which we will call sTDA*). Clearly the only two differences between sBSE and sTDA* are the use of sGW or DFT eigenvalues and the use of a screened Coulomb interaction or a rescaled bare Coulomb interaction. For solids or heterogeneous nanostructures, it is expected that the screening in sBSE provides a more accurate treatment of the electron-hole interaction.

Select eigenvalues of the sTDA* or sBSE matrices can be found by iterative eigensolvers, like the Davidson algorithm, that require only matrix-vector products and the $O(N^2)$ storage of trial vectors c_i^a . With the integral approximations (2) and (21), the sTDA* and sBSE matrix-vector product can be done with $O(N^2)$ storage in $O(N^3)$ time,

$$[\mathbf{Ac}]_{ia} = (E_a - E_i)c_i^a + \alpha \sum_{\mu} C'_{\mu i} C'_{\mu a} \sum_{\nu} J_{\mu \nu} \sum_{jb} C'_{\nu j} C'_{\nu b} c_j^b$$

$$- \sum_{\mu} C'_{\mu i} \sum_{\nu} C'_{\nu a} W_{\mu \nu} \sum_{j} C'_{\mu j} \sum_{b} C'_{\nu b} c_j^b$$
(23)

with intermediate formation as indicated. In fact, if only a few sBSE eigenvalues are desired and only $O(N^2)$ storage is available, then the calculation of the sGW eigenvalues to be used in the sBSE is more expensive than finding the few eigenvalues of the sBSE matrix. We note that the original sTDA method³⁹ employs an aggressive but accurate truncation of the excitation space followed by complete diagonalization. Formally, this incurs an $O(N^4)$ computational cost or higher, which is why we suggest the iterative diagonalization above that guarantees $O(N^3)$ computational scaling per eigenvalue. However, depending on system size and the number of eigenvalues desired, the walltime of the original truncation approach might be lower and can be straightforwardly used with

the sBSE matrix.

3 Results

All calculations (DFT, GW/BSE, sGW/sBSE, and sTDA*) were performed using a locally modified version of the PySCF software package ^{29,59,60} using the TZVP basis set. ⁶¹ DFT calculations used the B3LYP exchange-correlation functional unless stated otherwise.

3.1 Simplified GW

The performance of sGW is assessed with the first ionization potential (highest occupied molecular orbital energy) of the atoms and molecules in the GW100 test set, ¹⁵ using the published geometries; ⁶² the TZVP basis set is used for all atoms except I, Xe, and Rb for which the DZVP basis set is used. We assess the accuracy of sGW by comparing to *ab initio*, full-frequency GW calculations (i.e., without the plasmon pole approximation) using the same basis set.

We first address the evaluation of the static exchange part of the self-energy. As mentioned previously, it can be approximated by Eq. (2), Eq. (5), or calculated exactly, which is free when a hybrid functional is used in the DFT reference. Figure 1(a) compares the IPs from *ab initio* GW to those of sGW when approximate [Eq. (5)] or exact exchange matrix elements are used. With approximate exchange, the single free parameter β_K is optimized to minimize the mean absolute error (MAE) with respect to the *ab initio* GW calculations, which leads to $\beta_K = 0.46$; this value was found to be robust to the basis set or exchange-correlation functional used. This approximate treatment of exchange gives a reasonable estimate of the IP with a MAE of 1.81 eV (note that the IPs of the test set range from -25 to -3 eV). The use of the exact exchange integrals greatly increases the accuracy, giving a MAE of only 0.20 eV. These results reflect the fact that the static exchange part of the self-energy is significantly larger in magnitude than the dynamical correlation part. Figure 1(b) shows that sGW also gives good agreement with experimental IPs, ¹⁵ especially when exact exchange is used. We reiterate that because exact exchange matrix elements were

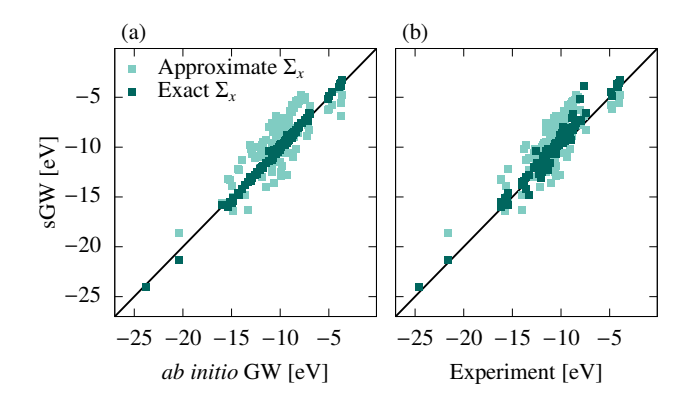


Figure 1: First ionization potential of the molecules in the GW100 set calculated by sGW@B3LYP compared to (a) *ab initio* GW@B3LYP results and (b) experiment, using an approximate (light) and exact (dark) bare exchange matrix element.

already computed in the DFT step, the sGW calculations with exact exchange have essentially the same cost as those with approximate exchange. We only expect a difference in timing when the parent DFT calculation uses a semilocal functional but, even in this case, the cost to calculate the correlation part of the self-energy still dominates. Therefore, for the rest of this study, the exact exchange part of the self-energy is used, but we will return to this point in Sec. 4.

Table 1 summarizes the MAE, mean signed error (MSE), and mean absolute relative error (MARE) of the sGW IPs compared to *ab initio* GW IPs and of both methods compared to experimental values. The GW and sGW calculations used PBE, PBE0, and B3LYP references; for PBE, we calculated the exact diagonal matrix element of the exchange operator after the SCF convergence. Calculations using the hybrid functionals PBE0 and B3LYP are about 0.2 eV more accurate than those with the PBE functional. The difference in the performance of the *ab initio* GW and sGW is marginal with MAREs of around 2%, indicating an accurate estimation of the correlation term of the self-energy by sGW. As will be demonstrated in Sec. 3.3, the cost of the sGW calculations is significantly smaller than that of the *ab initio* GW calculations.

3.2 Simplified BSE

Neutral excitation energies calculated by sTDA and sGW/sBSE are tested on a set of 28 organic molecules commonly known as Thiel's set, ^{64,65} using the published geometries in reference 64.

Figure 2 compares 97 singlet states and 51 triplet states calculated by sBSE to those calculated by *ab initio* BSE and to the best theoretical estimates from higher level methods proposed by Thiel and coworkers. 64,65 The *ab initio* BSE calculations are done using full-frequency GW eigenvalues, with *ab initio* static screening of the Coulomb interaction (i.e., without the plasmon-pole approximation), and without the Tamm-Dancoff approximation. The MAEs and MSEs are summarized in Table 2. The MAEs of singlet and triplet excitations calculated by sBSE with respect to *ab initio* BSE are 0.51 eV and 0.38 eV, respectively, which are similar to the errors exhibited by sGW, but the MAREs are larger (about 10%) simply because the excitation energies are smaller than IPs. The MAEs of singlet and triplet excitations calculated by sBSE with respect to the theoretical best estimates are 0.71 eV and 0.81 eV, respectively, which are similar to the errors exhibited by *ab initio* BSE. Once again we conclude that the performance difference between *ab initio* BSE and sBSE is marginal. Interestingly, sTDA* gives similar but smaller errors for both singlets and triplets when compared to the best theoretical estimates.

3.3 Applications

Having demonstrated the accuracy of the sGW/sBSE framework on benchmark sets of small molecules, we move on to study silicon clusters as a prototypical semiconductor nanomaterial. Specifically, we apply sGW/sBSE@B3LYP to hydrogen-passivated silicon clusters ranging from

Table 1: Mean absolute error (MAE), mean absolute relative error (MARE) and mean signed error (MSE) of the first ionization potential of the molecules in the GW100 test set with respect to *ab initio* GW and experimental values. Errors are in eV and exact exchange matrix elements were used in the sGW calculations.

	PBE		PBE0		B3LYP	
	GW	sGW	GW	sGW	GW	sGW
MAE wrt GW	-	0.23	-	0.19	-	0.20
MSE wrt GW	-	-0.01	-	-0.03	-	-0.04
MARE wrt GW	-	2.4%	-	1.9%	-	2.0%
MAE wrt Expt	0.89	0.93	0.68	0.69	0.72	0.72
MSE wrt Expt	0.85	0.84	0.57	0.53	0.62	0.58
MARE wrt Expt	8.8%	11.5%	6.8%	8.4%	7.1%	8.7%

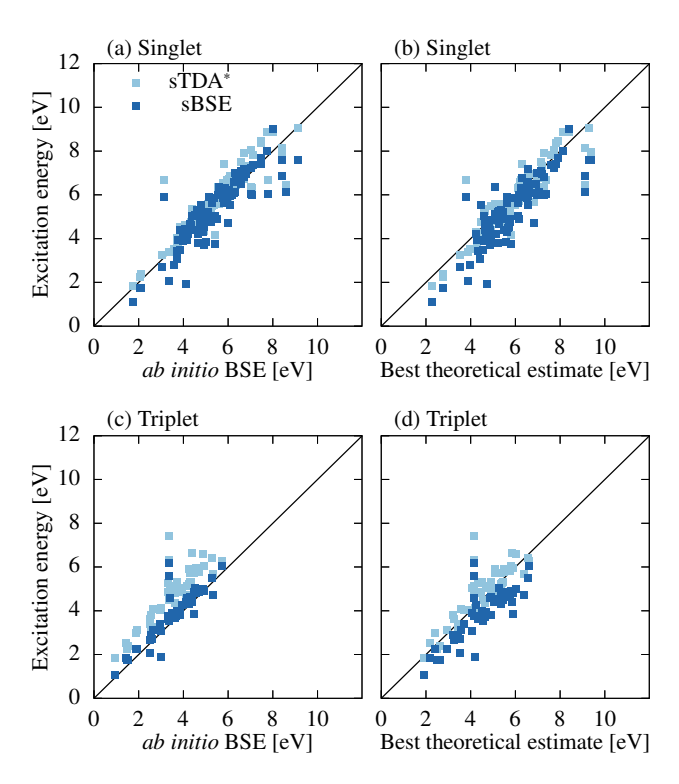


Figure 2: Singlet excitation energies of the 28 molecules in Thiel's set calculated by sBSE compared to (a) *ab initio* BSE results and (b) best theoretical estimates. Analogous results for triplet excitation energies are shown in (c) and (d).

SiH₄ to Si₁₈₁H₁₁₆, which has 2650 electrons and 4678 spatial orbitals. Calculations on larger clusters were limited by the cost of the initial B3LYP calculation. The structure of SiH₄ is from the GW100 set, ¹⁵ the structures of Si₅H₁₂ and Si₁₀H₁₆ are from PubChem, ⁶⁶ and the structures of larger clusters are from CSIRO Nanostructure Data Bank, ⁶⁷ without further geometry relaxation. In Fig. 3(a), we show the quasiparticle gap (calculated by DFT and sGW) and the first neutral excitation energy (calculated by sBSE, sTDA*, and the original sTDA³⁹) as a function of the cluster diameter, which is estimated by approximating the cluster as a sphere with a number density equal to that of bulk silicon (50 atoms/nm³). As expected, we see a large band gap renormalization from sGW and a large exciton binding energy from sBSE, both of which are reduced with increased cluster size.

For comparison, we show experimental photoluminescence energies from Ref. 68. The large system sizes accessible with sGW/sBSE allow us to compare directly to these experimental values. We see that the sBSE excitation energies are about 1 eV higher than experiment. Interestingly, we

find that the original sTDA and our modified sTDA* methods predict excitation energies that are only about 0.3 eV higher than experiment (and almost identical to one another, indicating that their technical differences are inconsequential). However, we emphasize that a direct comparison with experiment is complicated by potential differences in atomic structure as well as vibrational, finite-temperature, or environmental effects. The choice of DFT functional will also affect excitation energies, which we study in more detail in the next example.

Figure 3(b) shows the CPU time of each method as a function of number of electrons in the silicon clusters. In practice, most calculations are performed with some degree of parallelism using up to 32 cores; thus, while we report the total CPU time, the wall time can be significantly less. For sGW, we report the CPU time required per eigenvalue using the algorithm that requires only $O(N^2)$ storage, such that we expect $O(N^3)$ scaling, which is confirmed numerically. The savings afforded by our sGW algorithm enabled us to calculate about 2500 GW orbital energies on our largest system (with 2650 electrons and 4678 total orbitals) in about three days using a single 32-core node. The sBSE calculations were performed in a truncated space that included those orbitals with energies between 30 eV below the highest occupied orbital and 30 eV above the lowest unoccupied orbital. Again we report the CPU time required per eigenvalue, such that we expect $O(N^3)$ scaling, which is confirmed numerically. In practice, we were able to calculate 50 excitation energies on the largest nanocluster in less than an hour with less than 1 GB of memory. We note that the sBSE calculations are less expensive than the preceding sGW calculations.

Table 2: Mean absolute error (MAE), mean absolute relative error (MARE) and mean signed error (MSE) of singlet and triplet excitation energies of Thiel's set with respect to *ab initio* BSE and best theoretical estimates (BTE). Errors are in eV.

	Singlet			Triplet		
	BSE	sBSE	$sTDA^*$	BSE	sBSE	$sTDA^*$
MAE wrt BSE	-	0.51	0.47	-	0.38	1.22
MSE wrt BSE	-	-0.10	0.31	-	0.27	1.22
MARE wrt BSE	-	10.3%	9.1%	-	12.1%	38.0%
MAE wrt BTE	0.50	0.71	0.44	0.93	0.81	0.47
MSE wrt BTE	-0.46	-0.56	-0.15	-0.93	-0.66	0.29
MARE wrt BTE	9.2%	13.2%	8.0%	21.8%	18.5%	11.1%

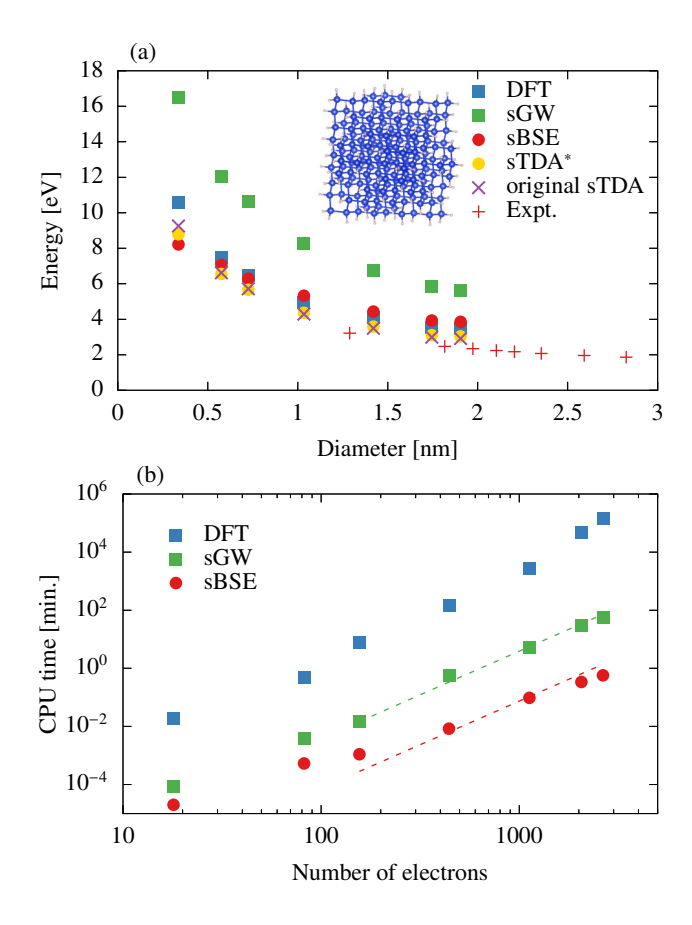


Figure 3: (a) Quasiparticle gap calculated by DFT (B3LYP) and sGW@B3LYP and first excitation energy calculated by sBSE, sTDA*, and original sTDA of silicon nanoclusters. Experimental results (plus signs) were determined in Ref. 68 by photoluminescence. Also shown is the molecular structure of the largest studied cluster, $Si_{181}H_{116}$, which has 2650 electrons and 4678 orbitals in the TZVP basis set. (b) CPU time required for DFT and CPU time required per eigenvalue for sGW and sBSE calculations. The sBSE calculations used a truncated set of orbitals. The dashed lines show N^3 power laws.

As a final class of example problems, we apply sGW/sBSE to study the optical properties of large organic molecules using four different DFT functionals as the starting point. In Fig. 4, we show the absorption spectra of a 192-atom organic dye molecule and a 126-atom chlorophyll-based donor-bridge-acceptor dyad, whose structures and experimental spectra are taken from Refs. 43 and 69, respectively. Calculations based on local functionals such as LDA and PBE fail to predict the characteristic peaks of both molecules. However, when starting from hybrid functionals, the agreement between sBSE and experiment is quite good considering that solvent effects and vibrational dynamics are neglected. Since PBE0 and B3LYP show similar performance (with

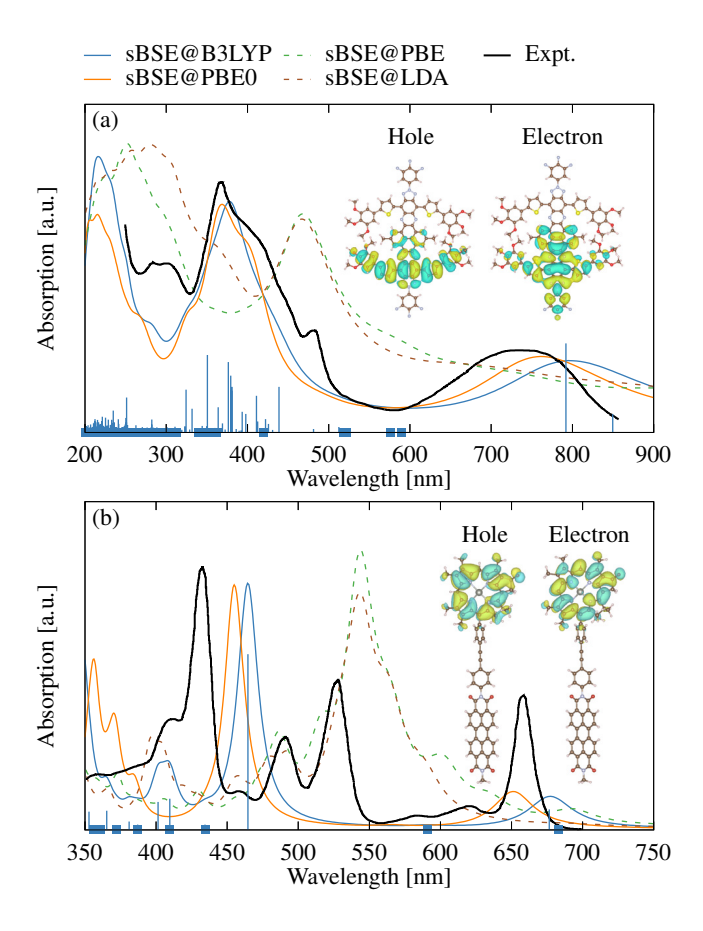


Figure 4: Absorption spectra of (a) an organic dye molecule and (b) a chlorophyll-based donor-bridge-acceptor molecule calculated using four different functionals. Blue vertical lines indicate the relative oscillator strength of each transition calculated by sGW/sBSE@B3LYP. Blue squares show the transitions with vanishing oscillator strength. Natural transition orbitals of the transitions at 792 nm (a) and 677 nm (b) are shown as insets.

PBE0 slightly better than B3LYP), the following analysis holds for both hybrid functionals.

As shown in Fig. 4(a), the organic dye molecule has a broad peak between 700 and 800 nm and strong peak at 360 nm; the sBSE predicts a slightly redshifted broad peak, but correctly predicts the strong peak at 360 nm, including its lineshape. As shown in Fig. 4(b), the chlorophyll molecule has two prototypical strong peaks, the so-called Q band and Soret band. The sBSE reproduces the Q band near 650 nm and the strong Soret band around 430 nm. However, we note that some transitions are spectroscopically dark at the equilibrium geometry but the experimental spectrum shows clear vibronic signatures, indicating the likely importance of nuclear dynamics for total agreement. Despite being a semiempirical method, sBSE yields a proper excited-state wavefunction, enabling

a variety of analyses. As an example, in Fig. 4, we show the largest-weight natural transition orbitals (NTOs)⁷⁰ of one low-lying transition of each molecule (NTOs are the electron-hole orbital pair that best represent the transition). Clearly, the NTOs show that the two analyzed excitations are relatively localized to specific regions of the molecules.

4 Conclusions and future work

We have presented the simplified GW and BSE methods, which we call sGW/sBSE. In addition to the plasmon-pole and static screening approximations, an approximate compression of the electron repulsion integrals is most responsible for the low cost of sGW/sBSE. The sGW/sBSE results are in good agreement with *ab initio* results as well as those of experiments or higher-level methods. In its present form, we expect that sGW/sBSE can facilitate rapid, semiquantitative calculations of charged and neutral excitations of large molecules and nanomaterials.

An obvious limitation of the present sGW/sBSE framework is its reliance on an initial *ab initio* DFT calculation, especially when hybrid functionals are used, as can be seen from Fig. 3(b). Future work will address the replacement of DFT with a semiempirical mean-field theory, similar to the combination of the extended tight-binding method (xTB) with the sTDA for extremely affordable calculations of excitation energies. Additionally, we plan to implement spin-orbit coupling and Brillouin zone sampling for periodic systems. More generally, sGW/sBSE could be made into a more *ab initio* method by pursuing similar structure through tensor decompositions or integral screening. Lastly, we believe that the sGW/sBSE framework could be used as an affordable testing ground for improvements to the GW/BSE formalism, such as self-consistency, vertex corrections, 71–74 or the combination of GW with dynamical mean-field theory. 75,76

Associated content

The data and code underlying this study are available from the corresponding author upon reasonable request.

Acknowledgements

This work was supported in part by the National Science Foundation under Grant No. OAC-1931321 (Y.C.) and by the National Science Foundation Graduate Research Fellowship under Grant No. DGE-1644869 (S.J.B.) We acknowledge computing resources from Columbia University's Shared Research Computing Facility project, which is supported by NIH Research Facility Improvement Grant 1G20RR030893-01, and associated funds from the New York State Empire State Development, Division of Science Technology and Innovation (NYSTAR) Contract C090171, both awarded April 15, 2010. The Flatiron Institute is a division of the Simons Foundation.

References

- (1) Hedin, L. New Method for Calculating the One-Particle Green's Function with Application to the Electron-Gas Problem. *Phys. Rev.* **1965**, *139*, A796–A823.
- (2) Strinati, G.; Mattausch, H. J.; Hanke, W. Dynamical Correlation Effects on the Quasiparticle Bloch States of a Covalent Crystal. *Phys. Rev. Lett.* **1980**, *45*, 290–294.
- (3) Hanke, W.; Sham, L. J. Many-particle effects in the optical spectrum of a semiconductor. *Phys. Rev. B* **1980**, *21*, 4656–4673.
- (4) Strinati, G.; Mattausch, H. J.; Hanke, W. Dynamical aspects of correlation corrections in a covalent crystal. *Phys. Rev. B* **1982**, *25*, 2867–2888.
- (5) Strinati, G. Effects of dynamical screening on resonances at inner-shell thresholds in semi-conductors. *Phys. Rev. B* **1984**, *29*, 5718–5726.
- (6) Hybertsen, M. S.; Louie, S. G. First-Principles Theory of Quasiparticles: Calculation of Band Gaps in Semiconductors and Insulators. *Phys. Rev. Lett.* **1985**, *55*, 1418–1421.

- (7) Hybertsen, M. S.; Louie, S. G. Electron correlation in semiconductors and insulators: Band gaps and quasiparticle energies. *Phys. Rev. B* **1986**, *34*, 5390–5413.
- (8) Albrecht, S.; Reining, L.; Sole, R. D.; Onida, G. Excitonic Effects in the Optical Properties. *Phys. Status Solidi* **1998**, *170*, 189–197.
- (9) Rohlfing, M.; Louie, S. G. Electron-hole excitations and optical spectra from first principles. *Phys. Rev. B* **2000**, *62*, 4927–4944.
- (10) Tiago, M. L.; Chelikowsky, J. R. First-principles GW–BSE excitations in organic molecules. *Solid State Commun.* **2005**, *136*, 333–337.
- (11) Faber, C.; Boulanger, P.; Attaccalite, C.; Duchemin, I.; Blase, X. Excited states properties of organic molecules: from density functional theory to the GW and Bethe–Salpeter Green's function formalisms. *Philos. Trans. Royal Soc. A* **2014**, *372*, 20130271.
- (12) Körbel, S.; Boulanger, P.; Duchemin, I.; Blase, X.; Marques, M. A. L.; Botti, S. Benchmark Many-Body GW and Bethe–Salpeter Calculations for Small Transition Metal Molecules. *J. Chem. Theory Comput.* 2014, 10, 3934–3943.
- (13) Bruneval, F.; Hamed, S. M.; Neaton, J. B. A systematic benchmark of the ab initio Bethe-Salpeter equation approach for low-lying optical excitations of small organic molecules. *J. Chem. Phys.* **2015**, *142*, 244101.
- (14) Jacquemin, D.; Duchemin, I.; Blase, X. Benchmarking the Bethe–Salpeter Formalism on a Standard Organic Molecular Set. *J. Chem. Theory Comput.* **2015**, *11*, 3290–3304.
- (15) van Setten, M. J.; Caruso, F.; Sharifzadeh, S.; Ren, X.; Scheffler, M.; Liu, F.; Lischner, J.; Lin, L.; Deslippe, J. R.; Louie, S. G.; Yang, C.; Weigend, F.; Neaton, J. B.; Evers, F.; Rinke, P. GW100: Benchmarking G0W0 for Molecular Systems. *J. Chem. Theory Comput.* 2015, 11, 5665–5687.

- (16) Caruso, F.; Dauth, M.; van Setten, M. J.; Rinke, P. Benchmark of GW Approaches for the GW100 Test Set. *J. Chem. Theory Comput.* **2016**, *12*, 5076–5087.
- (17) Knight, J. W.; Wang, X.; Gallandi, L.; Dolgounitcheva, O.; Ren, X.; Ortiz, J. V.; Rinke, P.; Körzdörfer, T.; Marom, N. Accurate Ionization Potentials and Electron Affinities of Acceptor Molecules III: A Benchmark of GW Methods. J. Chem. Theory Comput. 2016, 12, 615–626.
- (18) Rangel, T.; Hamed, S. M.; Bruneval, F.; Neaton, J. B. An assessment of low-lying excitation energies and triplet instabilities of organic molecules with an ab initio Bethe-Salpeter equation approach and the Tamm-Dancoff approximation. *J. Chem. Phys.* **2017**, *146*, 194108.
- (19) Foerster, D.; Koval, P.; Sánchez-Portal, D. An O(N3) implementation of Hedin's GW approximation for molecules. *J. Chem. Phys.* **2011**, *135*, 074105.
- (20) Deslippe, J.; Samsonidze, G.; Strubbe, D. A.; Jain, M.; Cohen, M. L.; Louie, S. G. BerkeleyGW: A massively parallel computer package for the calculation of the quasiparticle and optical properties of materials and nanostructures. *Comput. Phys. Commun.* 2012, 183, 1269–1289.
- (21) van Setten, M. J.; Weigend, F.; Evers, F. The GW-Method for Quantum Chemistry Applications: Theory and Implementation. *J. Chem. Theory Comput.* **2013**, *9*, 232–246.
- (22) Govoni, M.; Galli, G. Large Scale GW Calculations. J. Chem. Theory Comput. 2015, 11, 2680–2696.
- (23) Ljungberg, M. P.; Koval, P.; Ferrari, F.; Foerster, D.; Sánchez-Portal, D. Cubic-scaling iterative solution of the Bethe-Salpeter equation for finite systems. *Phys. Rev. B* **2015**, *92*, 075422.
- (24) Krause, K.; Klopper, W. Implementation of the Bethe-Salpeter equation in the TURBO-MOLE program. *J. Comput. Chem.* **2016**, *38*, 383–388.

- (25) Bruneval, F.; Rangel, T.; Hamed, S. M.; Shao, M.; Yang, C.; Neaton, J. B. molgw 1: Manybody perturbation theory software for atoms, molecules, and clusters. *Comput. Phys. Commun.* **2016**, 208, 149–161.
- (26) Wilhelm, J.; Golze, D.; Talirz, L.; Hutter, J.; Pignedoli, C. A. Toward GW Calculations on Thousands of Atoms. *J. Phys. Chem. Lett.* **2018**, *9*, 306–312.
- (27) Koval, P.; Ljungberg, M. P.; Müller, M.; Sánchez-Portal, D. Toward Efficient GW Calculations Using Numerical Atomic Orbitals: Benchmarking and Application to Molecular Dynamics Simulations. J. Chem. Theory Comput. 2019, 15, 4564–4580.
- (28) Liu, C.; Kloppenburg, J.; Yao, Y.; Ren, X.; Appel, H.; Kanai, Y.; Blum, V. All-electron ab initio Bethe-Salpeter equation approach to neutral excitations in molecules with numeric atom-centered orbitals. *J. Chem. Phys.* **2020**, *152*, 044105.
- (29) Zhu, T.; Chan, G. K.-L. All-Electron Gaussian-Based G0W0 for Valence and Core Excitation Energies of Periodic Systems. *J. Chem. Theory Comput.* **2021**, *17*, 727–741.
- (30) Bintrim, S. J.; Berkelbach, T. C. Full-frequency GW without frequency. *J. Chem. Phys.* **2021**, *154*, 041101.
- (31) Blase, X.; Duchemin, I.; Jacquemin, D. The Bethe–Salpeter equation in chemistry: relations with TD-DFT, applications and challenges. *Chem. Soc. Rev.* **2018**, *47*, 1022–1043.
- (32) Golze, D.; Dvorak, M.; Rinke, P. The GW Compendium: A Practical Guide to Theoretical Photoemission Spectroscopy. *Front. Chem.* **2019**, *7*, 377.
- (33) Blase, X.; Duchemin, I.; Jacquemin, D.; Loos, P.-F. The Bethe–Salpeter Equation Formalism: From Physics to Chemistry. *J. Phys. Chem. Lett.* **2020**, *11*, 7371–7382.
- (34) Elstner, M.; Porezag, D.; Jungnickel, G.; Elsner, J.; Haugk, M.; Frauenheim, T.; Suhai, S.; Seifert, G. Self-consistent-charge density-functional tight-binding method for simulations of complex materials properties. *Phys. Rev. B* **1998**, *58*, 7260–7268.

- (35) Hourahine, B.; Aradi, B.; Blum, V.; Bonafé, F.; Buccheri, A.; Camacho, C.; Cevallos, C.; Deshaye, M.; Dumitrică, T.; Dominguez, A.; others DFTB+, a software package for efficient approximate density functional theory based atomistic simulations. *J. Chem. Phys.* **2020**, *152*, 124101.
- (36) Grimme, S.; Bannwarth, C.; Shushkov, P. A Robust and Accurate Tight-Binding Quantum Chemical Method for Structures, Vibrational Frequencies, and Noncovalent Interactions of Large Molecular Systems Parametrized for All spd-Block Elements (Z = 1–86). *J. Chem. Theory Comput.* **2017**, *13*, 1989–2009.
- (37) Bannwarth, C.; Ehlert, S.; Grimme, S. GFN2-xTB—An accurate and broadly parametrized self-consistent tight-binding quantum chemical method with multipole electrostatics and density-dependent dispersion contributions. *J. Chem. Theory Comput.* **2019**, *15*, 1652–1671.
- (38) Bannwarth, C.; Caldeweyher, E.; Ehlert, S.; Hansen, A.; Pracht, P.; Seibert, J.; Spicher, S.; Grimme, S. Extended tight-binding quantum chemistry methods. *WIREs Comput. Mol. Sci.* **2020**, *11*.
- (39) Grimme, S. A simplified Tamm-Dancoff density functional approach for the electronic excitation spectra of very large molecules. *J. Chem. Phys.* **2013**, *138*, 244104.
- (40) Bannwarth, C.; Grimme, S. A simplified time-dependent density functional theory approach for electronic ultraviolet and circular dichroism spectra of very large molecules. *Computational and Theoretical Chemistry* **2014**, *1040*, 45–53.
- (41) Niehaus, T. A.; Suhai, S.; Della Sala, F.; Lugli, P.; Elstner, M.; Seifert, G.; Frauenheim, T. Tight-binding approach to time-dependent density-functional response theory. *Phys. Rev. B* **2001**, *63*, 085108.
- (42) Trani, F.; Scalmani, G.; Zheng, G.; Carnimeo, I.; Frisch, M. J.; Barone, V. Time-Dependent Density Functional Tight Binding: New Formulation and Benchmark of Excited States. *J. Chem. Theory Comput.* **2011**, *7*, 3304–3313.

- (43) Grimme, S.; Bannwarth, C. Ultra-fast computation of electronic spectra for large systems by tight-binding based simplified Tamm-Dancoff approximation (sTDA-xTB). *J. Chem. Phys.* **2016**, *145*, 054103.
- (44) Asadi-Aghbolaghi, N.; Ruger, R.; Jamshidi, Z.; Visscher, L. TD-DFT+ TB: An efficient and fast approach for quantum plasmonic excitations. *J. Phys. Chem. C* **2020**, *124*, 7946–7955.
- (45) de Wergifosse, M.; Grimme, S. Perspective on Simplified Quantum Chemistry Methods for Excited States and Response Properties. *The Journal of Physical Chemistry A* **2021**, *125*, 3841–3851.
- (46) Nishimoto, K.; Mataga, N. Electronic structure and spectra of some nitrogen heterocycles. *Z. Phys. Chem.* **1957**, *12*, 335–338.
- (47) Ohno, K. Some remarks on the Pariser-Parr-Pople method. *Theor. Chim. Acta* **1964**, 2, 219–227.
- (48) Klopman, G. A semiempirical treatment of molecular structures. II. Molecular terms and application to diatomic molecules. *J. Am. Chem. Soc.* **1964**, *86*, 4550–4557.
- (49) Whitten, J. L. Coulombic potential energy integrals and approximations. *J. Chem. Phys.* **1973**, 58, 4496–4501.
- (50) Vahtras, O.; Almlöf, J.; Feyereisen, M. Integral approximations for LCAO-SCF calculations. *Chem. Phys. Lett.* **1993**, *213*, 514–518.
- (51) Feyereisen, M.; Fitzgerald, G.; Komornicki, A. Use of approximate integrals in ab initio theory. An application in MP2 energy calculations. *Chem. Phys. Lett.* **1993**, 208, 359–363.
- (52) Werner, H.-J.; Manby, F. R.; Knowles, P. J. Fast linear scaling second-order Møller-Plesset perturbation theory (MP2) using local and density fitting approximations. *J. Chem. Phys.* **2003**, *118*, 8149–8160.

- (53) Ren, X.; Rinke, P.; Blum, V.; Wieferink, J.; Tkatchenko, A.; Sanfilippo, A.; Reuter, K.; Scheffler, M. Resolution-of-identity approach to Hartree–Fock, hybrid density functionals, RPA, MP2 and GWwith numeric atom-centered orbital basis functions. *New J. Phys.* 2012, 14, 053020.
- (54) Wilhelm, J.; Ben, M. D.; Hutter, J. GW in the Gaussian and Plane Waves Scheme with Application to Linear Acenes. *J. Chem. Theory Comput.* **2016**, *12*, 3623–3635.
- (55) Hohenstein, E. G.; Parrish, R. M.; Martínez, T. J. Tensor hypercontraction density fitting. I. Quartic scaling second- and third-order Møller-Plesset perturbation theory. J. Chem. Phys. 2012, 137, 044103.
- (56) Jacquemin, D.; Duchemin, I.; Blondel, A.; Blase, X. Benchmark of Bethe-Salpeter for Triplet Excited-States. *J. Chem. Theory Comput.* **2017**, *13*, 767–783.
- (57) von der Linden, W.; Horsch, P. Precise quasiparticle energies and Hartree-Fock bands of semiconductors and insulators. *Phys. Rev. B* **1988**, *37*, 8351.
- (58) Larson, P.; Dvorak, M.; Wu, Z. Role of the plasmon-pole model in the GWapproximation. *Phys. Rev. B* **2013**, 88, 125205.
- (59) Sun, Q.; Berkelbach, T. C.; Blunt, N. S.; Booth, G. H.; Guo, S.; Li, Z.; Liu, J.; McClain, J. D.; Sayfutyarova, E. R.; Sharma, S.; others PySCF: the Python-based simulations of chemistry framework. *WIREs Comput. Mol. Sci.* **2018**, 8, e1340.
- (60) Sun, Q.; Zhang, X.; Banerjee, S.; Bao, P.; Barbry, M.; Blunt, N. S.; Bogdanov, N. A.; Booth, G. H.; Chen, J.; Cui, Z.-H.; Eriksen, J. J.; Gao, Y.; Guo, S.; Hermann, J.; Hermes, M. R.; Koh, K.; Koval, P.; Lehtola, S.; Li, Z.; Liu, J.; Mardirossian, N.; McClain, J. D.; Motta, M.; Mussard, B.; Pham, H. Q.; Pulkin, A.; Purwanto, W.; Robinson, P. J.; Ronca, E.; Sayfutyarova, E. R.; Scheurer, M.; Schurkus, H. F.; Smith, J. E. T.; Sun, C.; Sun, S.-N.; Upadhyay, S.; Wagner, L. K.; Wang, X.; White, A.; Whitfield, J. D.; Williamson, M. J.;

- Wouters, S.; Yang, J.; Yu, J. M.; Zhu, T.; Berkelbach, T. C.; Sharma, S.; Sokolov, A. Y.; Chan, G. K.-L. Recent developments in the PySCF program package. *J. Chem. Phys.* **2020**, *153*, 024109.
- (61) Schäfer, A.; Huber, C.; Ahlrichs, R. Fully optimized contracted Gaussian basis sets of triple zeta valence quality for atoms Li to Kr. *J. Chem. Phys.* **1994**, *100*, 5829–5835.
- (62) Structure files are available at https://github.com/setten/GW100. Accessed March 4, 2022.
- (63) Godbout, N.; Salahub, D. R.; Andzelm, J.; Wimmer, E. Optimization of Gaussian-type basis sets for local spin density functional calculations. Part I. Boron through neon, optimization technique and validation. *Can. J. Chem.* **1992**, *70*, 560–571.
- (64) Schreiber, M.; Silva-Junior, M. R.; Sauer, S. P.; Thiel, W. Benchmarks for electronically excited states: CASPT2, CC2, CCSD, and CC3. *J. Chem. Phys.* **2008**, *128*, 134110.
- (65) Silva-Junior, M. R.; Schreiber, M.; Sauer, S. P.; Thiel, W. Benchmarks for electronically excited states: Time-dependent density functional theory and density functional theory based multireference configuration interaction. *J. Chem. Phys.* 2008, 129, 104103.
- (66) National Center for Biotechnology Information. 2021; PubChem Compound Summary for CID 71353974 and 101946798. https://pubchem.ncbi.nlm.nih.gov. Accessed July 1, 2021.
- (67) Wilson, H. F.; McKenzie-Sell, L.; Barnard, A. S. Shape dependence of the band gaps in luminescent silicon quantum dots. *J. Mater. Chem. C* **2014**, 2, 9451–9456.
- (68) Wolkin, M.; Jorne, J.; Fauchet, P.; Allan, G.; Delerue, C. Electronic states and luminescence in porous silicon quantum dots: the role of oxygen. *Phys. Rev. Lett.* **1999**, 82, 197.
- (69) Huang, G.-J.; Harris, M. A.; Krzyaniak, M. D.; Margulies, E. A.; Dyar, S. M.; Lindquist, R. J.; Wu, Y.; Roznyatovskiy, V. V.; Wu, Y.-L.; Young, R. M.; others Photoinduced Charge and Energy Transfer within meta-and para-Linked Chlorophyll a-perylene-3, 4: 9, 10-bis (dicarboximide) Donor–Acceptor Dyads. *J. Phys. Chem. B* 2016, 120, 756–765.

- (70) Martin, R. L. Natural transition orbitals. *J. Chem. Phys.* **2003**, *118*, 4775–4777.
- (71) Shishkin, M.; Marsman, M.; Kresse, G. Accurate Quasiparticle Spectra from Self-ConsistentGWCalculations with Vertex Corrections. *Phys. Rev. Lett.* **2007**, *99*, 246403.
- (72) Romaniello, P.; Guyot, S.; Reining, L. The self-energy beyond GW: Local and nonlocal vertex corrections. *J. Chem. Phys.* **2009**, *131*, 154111.
- (73) Maggio, E.; Kresse, G. GW Vertex Corrected Calculations for Molecular Systems. *J. Chem. Theory Comput.* **2017**, *13*, 4765–4778.
- (74) Lewis, A. M.; Berkelbach, T. C. Vertex Corrections to the Polarizability Do Not Improve the GW Approximation for the Ionization Potential of Molecules. *J. Chem. Theory Comput.* 2019, 15, 2925–2932.
- (75) Biermann, S.; Aryasetiawan, F.; Georges, A. First-Principles Approach to the Electronic Structure of Strongly Correlated Systems: Combining the GWApproximation and Dynamical Mean-Field Theory. *Phys. Rev. Lett.* **2003**, *90*, 086402.
- (76) Zhu, T.; Chan, G. K.-L. Ab Initio Full Cell GWDMFT for Correlated Materials. *Phys. Rev. X* **2021**, *11*, 021006.